Heat Shock Protein-90 Inhibition Alters Activation of Pancreatic Stellate Cells and Enhances the Efficacy of PD-1 Blockade in Pancreatic Cancer

Yuchen Zhang[1,2], Michael B. Ware[1], Mohammad Y. Zaidi[3], Amanda N. Ruggieri[1], Brian M. Olson[1], Hannah Komar[1], Matthew R. Farren[1], Ganji Purnachandra Nagaraju[1], Chao Zhang[4], Zhengjia Chen[5], Juan M. Sarmiento[3], Rafi Ahmed[6], Shishir K. Maithel[3], Bassel F. El-Rayes[1], and Gregory B. Lesinski[1]

ABSTRACT

Pancreatic ductal adenocarcinoma (PDAC) has a prominent fibrotic stroma, which is a result of interactions between tumor, immune and pancreatic stellate cells (PSC), or cancer-associated fibroblasts (CAF). Targeting inflammatory pathways present within the stroma may improve access of effector immune cells to PDAC and response to immunotherapy. Heat shock protein-90 (Hsp90) is a chaperone protein and a versatile target in pancreatic cancer. Hsp90 regulates a diverse array of cellular processes of relevance to both the tumor and the immune system. However, to date the role of Hsp90 in PSC/CAF has not been explored in detail. We hypothesized that Hsp90 inhibition would limit inflammatory signals, thereby reprogramming the PDAC tumor microenvironment to enhance sensitivity to PD-1 blockade. Treatment of immortalized and primary patient PSC/CAF with the Hsp90 inhibitor XL888 decreased IL6, a key cytokine that orchestrates immune changes in PDAC at the transcript and protein level *in vitro*. XL888 directly limited PSC/CAF growth and reduced Jak/STAT and MAPK signaling intermediates and alpha-SMA expression as determined via immunoblot. Combined therapy with XL888 and anti–PD-1 was efficacious in C57BL/6 mice bearing syngeneic subcutaneous (Panc02) or orthotopic (KPC-Luc) tumors. Tumors from mice treated with both XL888 and anti–PD-1 had a significantly increased $CD8^+$ and $CD4^+$ T-cell infiltrate and a unique transcriptional profile characterized by upregulation of genes associated with immune response and chemotaxis. These data demonstrate that Hsp90 inhibition directly affects PSC/CAF *in vitro* and enhances the efficacy of anti–PD-1 blockade *in vivo*.

Introduction

There is an urgent need for effective therapeutic approaches for patients with pancreatic ductal adenocarcinoma (PDAC). Prognosis for patients with PDAC is dismal, with 5-year survival of only 10% in the United States (1). The incidence of PDAC is also increasing and is predicted to emerge as the second leading cause of cancer-related death by the year 2030 (2). Unfortunately, only incremental advances in the efficacy of chemotherapy approaches have been observed for PDAC, and in contrast to other tumor types, Abs targeting immune checkpoint molecules rarely provide clinical benefit.

One prominent feature of PDAC that can thwart effective T-cell–mediated antitumor immune responses is a dense, desmoplastic stroma (3). A particularly hostile environment emerges as a result of complex interactions between multiple cell types including tumor cells, immunosuppressive cells, and inflammatory cancer-associated fibroblasts (CAF) that can arise from "pancreatic stellate cells" (PSC; refs. 3–9). This fibrotic, cancerous tissue is particularly adept at producing inflammatory cytokines and chemokines that alter trafficking and phenotype of cells in the tumor microenvironment (TME). Abundant factors including IL6, IL1α, and TGFβ among others lead to sustained activation of inflammatory signaling pathways across multiple cellular components of the TME (9–14).

Although inflammatory signaling pathways in the PDAC TME are attractive targets, there remains a high level of redundancy making this approach difficult. However, there are key nodes that may simultaneously regulate multiple factors across cellular compartments. Among these are Hsp90, a key chaperone protein that regulates a diverse array of cellular processes relevant to both the tumor and immune system (15, 16). Inhibition of Hsp90 has direct effects on tumor cells including enhanced tumor antigen expression, class I MHC upregulation, and inflammatory cytokine production (15–18). These properties are likely mediated by the ability of Hsp90 inhibitors to interfere with activated inflammatory pathways including Jak/STAT and NF-κB (17–20). There has been renewed interest in targeting Hsp90 in recent years, resulting in novel small molecules that are under investigation in early phase clinical trials (21, 22). This has invigorated investigation of Hsp90 as a therapeutic target, despite early trials in PDAC marked by poor tolerability and limited efficacy with early generation inhibitors such as 17-AAG (23). Importantly, the availability of potent, well-tolerated Hsp90 inhibitors ready for clinical use represents a viable means to simultaneously modulate tumor, stromal, and immune compartments in the PDAC TME.

In this report, we address the hypothesis that Hsp90 inhibition limits inflammatory signals in the PDAC TME, resulting in enhanced efficacy of PD-1 blockade. We demonstrate Hsp90 inhibition with

[1]Department of Hematology and Medical Oncology, Winship Cancer Institute of Emory University, Atlanta, Georgia. [2]Department of Oncology, the First Affiliated Hospital of Xi'an Jiaotong University, Shaanxi, China. [3]Department of Surgery, Winship Cancer Institute of Emory University, Atlanta, Georgia. [4]Department of Biostatistics, Winship Cancer Institute of Emory University, Atlanta, Georgia. [5]Division of Epidemiology and Biostatistics, University of Illinois at Chicago, Chicago, Illinois. [6]Emory Vaccine Center, Atlanta, Georgia.

Note: Supplementary data for this article are available at Molecular Cancer Therapeutics Online (http://mct.aacrjournals.org/).

Corresponding Authors: Gregory B. Lesinski, Winship Cancer Institute of Emory University, 1365 Clifton Road NE, Atlanta, GA 30322. Phone: 404-778-3072; Fax: 404-778-5520; E-mail: gregory.b.lesinski@emory.edu; and Bassel F. El-Rayes. Phone: 404-778-1900; E-mail: bassel.el-rayes@emoryhealthcare.org

Mol Cancer Ther 2021;20:150–60

doi: 10.1158/1535-7163.MCT-19-0911

XL888, a clinically relevant small molecule, limits an activated phenotype of PSC/CAF. These *in vitro* data suggest PSC/CAF may be a cellular target affected by Hsp90 inhibition. Further results indicate that Hsp90 inhibition enhances *in vivo* efficacy in murine PDAC models when paired with Abs targeting PD-1. Finally, tumors from mice treated with the combination of XL888 and anti–PD-1 had increased $CD8^+$ and $CD4^+$ T-cell infiltration and differentially expressed genes related to chemokine and chemokine receptor expression. These novel preclinical data identify new cellular targets of Hsp90 inhibition and support further investigation into this treatment combination for therapy of advanced PDAC.

Materials and Methods

Cell lines and reagents

The heat shock protein 90 inhibitor XL888 (A11251) was purchased from Adooq Bioscience. The chemical structure for XL888 has been previously published (21). Murine Ab to PD-1 (Clone RMP1–14) and isotype control rat IgG2 (Clone 2A3) for *in vivo* studies were purchased from BioXcell. The murine pancreatic cancer cell line Panc02 was provided by Dr. Shari Pilon-Thomas (H. Lee Moffitt Cancer Center, Tampa, FL). KPC-Luc cells were provided by Dr. Craig Logsdon (M.D. Anderson Cancer Center, Houston, TX). These cells are derived from KPC mice ($Kras^{LSL\text{-}G12D}$, $Trp53^{-/-}$, and PDX-1-Cre) and transfected with enhanced firefly luciferase as described (24). Human pancreatic fibroblast (HPF) cells were purchased from Vitro Biopharma. Panc02, KPC-Luc, and HPF cells were cultured in DMEM (Gibco) with 10% FBS (Gibco) and antibiotic (Gibco). The MT-5 ($Kras^{LSL-G12D}$, $Trp53^{LSL-R270H}$) cell line was a gift from Dr. David Tuveson (Cold Spring Harbor Laboratory) and grown in RPMI-1640 (Gibco) with 10% FBS (Gibco) and antibiotics (Gibco). The human HPAC cell line was purchased from the ATCC and cultured in DMEM/F12 Medium (Gibco) with 10% FBS (Gibco), antibiotic (Gibco), 0.002 mg/mL insulin (Sigma-Aldrich), 0.005 mg/mL transferrin (Sigma-Aldrich), 40 ng/mL hydrocortisone (Sigma-Aldrich), and 10 ng/mL epidermal growth factor.

PSC/CAF isolation and culture

The human pancreatic cancer–associated stellate cell line h-iPSC-PDAC-1 was generated as previously described (25). Primary human PSC/CAF were isolated from resected pancreatic tumors in accordance with an Institutional Review Board–approved protocol at the Winship Cancer Institute of Emory University on deidentified tissue as described (12). Briefly, freshly resected pancreatic tissue was dissected into 1 mm^3 pieces, plated in uncoated wells with DMEM + 10% FBS and antibiotics, and incubated for 2 to 3 weeks to allow for PSC/CAF outgrowth and validation as described (25).

RNA extraction and real-time PCR

The h-iPSC-PDAC-1 cells were plated and treated with various concentration doses of XL888 for 24 hours, and total RNA was extracted using TRIzol Reagent (Invitrogen, 15596018) following the manufacturer's protocol. Total RNA was transcribed into cDNA according to the manufacturer's protocol using the iScript cDNA Synthesis Kit (Bio rad, 1708890). The *Power* SYBR Green PCR Master Mix reaction system (4367659) from Thermo Fisher Scientific was used to determine the mRNA level of IL6 with the primers 5′-GCAGAAAAAGGCAAAGAATC-3′(forward) and 5′-CTACATTT-GCCGAAGAGC-3′(reverse). GAPDH served as an internal control using the primers 5′-CTTTTGCGTCGCCAG-3′(forward) and 5′-TTGATGGCAACAATATCCAC-3′(reverse). The expression level of mRNA was quantitated using Applied Biosystems 7500 Fast Real-Time PCR System (Thermo Fisher Scientific) using the delta Ct method.

Protein extraction and Western blots

Following a 48-hour treatment with XL888, cells were collected and protein was extracted using RIPA lysis buffer together with 1% phosphatase inhibitor and 1% protease inhibitor. The Pierce BCA Protein Assay Kit (23227) from Thermo Fisher Scientific was used to determine protein concentration. Western blots were performed as described (25). Primary Abs for pSTAT3 (9145 L), STAT3 (4904 S), pERK (4377 S), tERK (4695 S), Hsp27 (50353), Hsp70 (4872), β-actin (4967 S) and secondary anti-Rabbit (7074 S), or anti-Mouse (7076 S) Abs were purchased from Cell Signaling Technology, Inc. Primary Ab for α-SMA (MA137027) was purchased from Thermo Fisher Scientific, Inc. Primary Ab for murine PD-L1 was purchased from Abcam (ab233482).

ELISA

Cell supernatants were collected following a-48 hour treatment with XL888. Human LIF DuoSet (DY7734–05) and human IL6 Duoset (DY206) were purchased from R&D Systems Inc. to measure cytokine expression following the manufacturers' protocol.

Oil Red "O" staining

h-iPSC-PDAC-1 cells were plated into chamber slides (Nalgene Nunc International) and treated with XL888 or 10 μmol/L al-trans retinoic acid (R2625, Sigma Aldrich). Forty-eight hours later, cells were fixed with 4% formalin in PBS for 30 minutes. Next cells were stained with Oil Red O (1320–06–5) from Sigma-Aldrich after incubation with 60% isopropanol for 5 minutes. VECTOR Hematoxylin QS (H-3404) from Vector Laboratories was used to stain the nuclear. Cells were then rinsed with tap water and mounted with mounting media. Images at 20x magnification were captured under the light microscope (Zeiss Axioplan 2) and analyzed using Fiji imageJ (GitHub) to figure out the area % of the lipid droplet.

MTT assay

Cells were grown in 96-well plates and treated with increasing concentrations of XL888. Following a 72-hour incubation, 10 μL MTT reagent (30–1010K, ATCC) was added to each well, and cells were incubated for 2 to 3 hours at 37°C with 5% CO_2. After removal of media, 200 μL of DMSO was added per well, and the absorbance was measured using a Synergy H1 plate reader (BioTek) at wave 595 nm. For these assays, all cells were plated in triplicate for each experimental condition.

Isolation and viability assay of human blood cells

Peripheral blood mononuclear cells (PBMC) were isolated using Ficoll-Paque (Amersham) from the blood of healthy adult donors as described (26). PBMCs were plated into 6-well plates at a density of 1×10^6 cells/well. The next day, different concentrations of XL888 were added, and after 48 hours, PBMCs were counted under the microscope after staining with Trypan Blue Solution 0.4% (15250061, Gibco).

Colony formation assays

Cells were trypsinized into a single-cell suspension and plated into 12-well plates at a low density (100–200 cells/well). XL888 was added the following day once cells were adherent and media were changed every 2 days. Following 10 to 14 days, cells were fixed with 4% formalin for 30 minutes at room temperature and stained with 0.5% Crystal

Violet (C3886, Sigma Aldrich) for 30 minutes. The number of colonies which contained more than 50 cells was counted via light microscopy.

In vivo experiments

All animal studies were conducted in accordance with a protocol approved by the Emory University Institutional Animal Care and Use Committee (IACUC). For s.c. tumor efficacy studies, 4- to 6-week-old female C57BL/6 mice (n = 6–7 mice per treatment group) were injected s.c. with 5×10^5 Panc02 cells in the right flank. Once tumors were palpable after 7 days, mice were either randomized to treatment with vehicle (10 mmol/L HCl, oral), XL888 (62.5 mg/kg, oral), anti–PD-1 (200 μg/mouse, intraperitoneal), or combined therapy with XL888 and anti–PD-1. Animals in vehicle or XL888 groups also received isotype control Ab (200 μg/mouse, intraperitoneal). All agents were administered for 2 weeks, 3 times per week, together with the measurement of the tumor volume. The dose of XL888 in this study was based on prior reports that have characterized its pharmacokinetic and pharmacodynamic properties (21). For orthotropic tumor efficacy studies, 6- to 8-week-old female C57BL/6 mice (n = 9 mice per treatment group) were injected with 2×10^5 KPC-Luc cells in 20 μL 1:1 PBS and Matrigel Matrix (354263, Discovery Labware, Inc.) into the tail of the pancreas and randomized into the treatment groups as indicated above (27). At days 7, 14, and 21 following injection, tumor progression was analyzed by bioluminescent imaging via the IVIS system. The study was terminated at day 21 where mice were euthanized via CO_2 inhalation followed by cardiac puncture as per IACUC-approved protocol. Following euthanasia, tumor weight was recorded, and tissues were preserved or freshly processed for subsequent biomarker analyses.

IHC analysis

Tumors from both s.c. and orthotopic efficacy studies were formalin-fixed, embedded in paraffin, and subjected to IHC analysis via staining with Abs directed against CD8 (Abcam, ab203035), αSMA (Santa Cruz Biotechnology, A1218), pSTAT3 (Cell Signaling Technology, Inc., 9145L), CD11c (Abcam, ab33483), CD45R/B220 (Fisher Scientific, BDB557390), and F4/80 (Abcam, ab100790). For analysis, images were acquired at 10x and 20x magnification (approximately 5–25 pictures per mouse depending on the size of the tumor) and captured using NDP.View2 software (Hamamatsu Photonics K.K.). Pictures for the staining of pSTAT3 and CD8 were analyzed by Fiji ImageJ (GitHub) to quantify the percentage of positive cells or the count of the positive cells. CellProfiler (Broad institute, Cambridge, MA) was used to analyze the αSMA staining pictures (28, 29). Qupath was used to quantify the staining for CD11c, B220, and F4/80. Orthotopic tumors were also stained for DAPI (Perkin Elmer), CD4 (Abcam, ab183685), and FOXP3 (Novus Biologicals, NB100–39002) and then visualized using a Vectra Polaris immunofluorescent whole slide scanner. Qupath was used to quantify the number of $CD4^+FOXP3^-$ and $CD4^+FOXP3^+$ cells per cm^2 tissue (30).

Nanostring gene expression analysis

RNA was isolated from representative tumors (n = 3/treatment group) from the orthotopic efficacy study using the Omega E.Z.N.A. FFPE Kit (Omega Bio-Tek) following the manufacturer's protocol, and quality was assessed using the Agilent 2100 bioanalyzer. Purified RNA underwent nanostring analysis using the nCounter Nanostring PanCancer Immune Profiling Panel (Nanostring Technologies). Pathway analysis was performed using Metacore (Clarivate Analytics) based on the list of differentially expressed genes.

Biostatistics

Data from densitometry analysis of Western blots, ELISA, MTT assay, and colony formation assays were analyzed using one-way ANOVA with P value < 0.05 as their significance, followed by a t test for multiple comparisons. For *in vivo* studies in mice bearing subcutaneous tumors, a mixed model was used to test for significant differences in longitudinal tumor volume across the four different treatment groups, followed by a pairwise group comparison in longitudinal tumor volume. For bioluminescence imaging (BLI) data in orthotopic tumors, linear mixed models were performed to test for significant change over time and for significant difference among treatment groups. Significance level was set at 0.05. The Kruskal–Wallis test was used to test for overall difference between groups for tumor weight, and IHC stains including αSMA, pSTAT3, CD4, and CD8, followed by a t test for multiple comparisons. The SAS9.4 statistical package (SAS Institute, Inc.) was used for data analysis.

Results

Inhibition of Hsp90 with XL888 limits an activated phenotype in PSC/CAF

We postulated that Hsp90 inhibitors can modulate PDAC stromal components that affect immunity. Although the ability of Hsp90 inhibitors to limit viability of PDAC has been documented in the literature (20, 31–38), the impact of these targeted agents on the biology of PSC/CAF has not been interrogated. Similar to PDAC tumor cell lines, immunoblot analysis revealed abundant Hsp90 expression in immortalized (h-iPSC-PDAC-1) or primary patient-derived (SC37) PDAC-associated PSC/CAF cultures. Hsp90 expression was significantly greater in h-iPSC-PDAC-1 ($P = 0.047$) and SC37 ($P = 0.014$) as compared with normal HPFs (**Fig. 1A** and **B**). h-iPSC-PDAC-1 cells were sensitive to the growth-inhibitory effects of XL888 (**Fig. 1C**). More detailed analysis revealed that XL888 exposure induced a concentration-dependent decrease in αSMA expression in h-iPSC-PDAC-1, a marker synonymous with an activated myofibroblast phenotype in PSC/CAF (**Fig. 1D**; Supplementary Fig. S1A). Consistent with the known chaperone activity of Hsp90, XL888 treatment also decreased phosphorylation of signaling pathways including ERK, STAT3, and upregulated Hsp27 and Hsp70, two well-characterized biomarkers of Hsp90 inhibition (**Fig. 1D**; Supplementary Fig. S1B–S1E). Oil Red O staining of h-iPSC-PDAC-1 cells following 48-hour exposure to XL888 further verified intracellular accumulation of lipid droplets, in a manner comparable with retinoic acid treatment as a positive control (**Fig. 1E**). Similar effects of XL888 on cell viability and activation phenotype were evident in primary PSC/CAF isolated from patients (**Fig 2A** and **B**), whereas less of an effect was observed on normal cell types with an inherently lower proliferation rate including HPFs or healthy donor PBMCs (**Fig. 2C–E**). Activated PSC/CAF produce an array of inflammatory cytokines including IL6 that facilitate immune-suppressive features of the TME (9–14). Consistent with a dampened activation, XL888 treatment led to significant reduction of IL6 in culture supernatants of h-iPSC-PDAC-1 cells (**Fig. 3A**). Downregulation of IL6 in response to XL888 occurred at the transcriptional level as determined by PCR at doses that did not induce reduced viability at later time points (**Fig. 3B**).

Inhibition of Hsp90 enhances the *in vivo* efficacy of anti–PD-1 blockade

The ability of XL888 to limit activation of stromal cells suggests it may represent a unique approach to modulating the tumor-immune

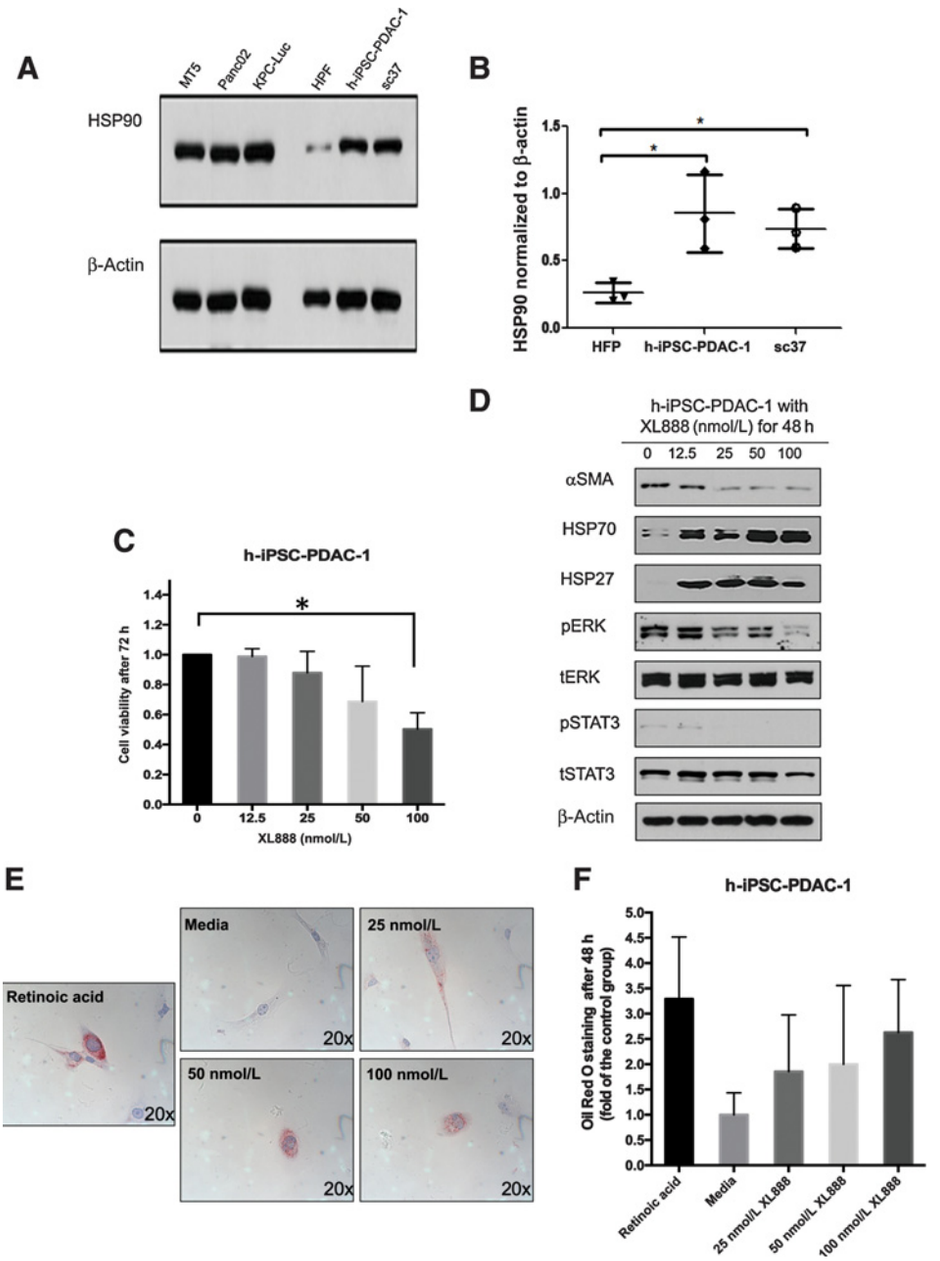

Figure 1.

Hsp90 inhibition limits activation of PSC/CAF. **A,** Immunoblot analysis of Hsp90 expression in a panel of murine PDAC cell lines (MT5, Panc02, and KPC-Luc), normal HPFs, immortalized PDAC-derived human PSC/CAF (h-iPSC-PDAC-1), and a primary PDAC patient–derived PSC/CAF culture (SC37). **B,** Densitometry analysis from $n = 3$ biological replicate blots. MTT assay (**C**) and immunoblot (**D**) of h-iPSC-PDAC-1 cells treated with increasing concentrations of XL888. **E–F,** Oil Red O staining of h-iPSC-PDAC-1 cells following treatment for 48 hours with XL888. Al-trans retinoic acid–treated cells served as a biological-positive control. For immunoblot analysis, β-actin served as a loading control. Error bars, SD of $n = 3$ biological replicates; *, $P < 0.05$.

microenvironment. Therefore, we first examined the ability of this agent to limit subcutaneous growth of panc02 tumors when administered in combination with PD-1–targeted Abs. Although single agent XL888 and anti–PD-1 Ab alone led to a modest inhibition of tumor growth rate, the combination of these agents led to a significant growth inhibition *in vivo* (**Fig. 4A**). Importantly, the regimen was well-tolerated and did not result in acute toxicity as evidenced by any reduction in body weight (**Fig. 4B**). Consistent with the reduced rate of growth inhibition, the end study weight of tumors from mice treated with XL888 and anti–PD-1 Ab combined was significantly lower than all other treatment groups (**Fig. 4C**). *In vitro* MTT assay, immunoblot, and colony formation assay data indicate that both murine (Panc02, MT-5, and KPC-Luc) and human (HPAC) cell lines were sensitive to the direct actions of XL888 (Supplementary Figs. S3 and S4). Taken together, these data indicate a portion of the antitumor efficacy of this combination was likely due to direct action on the tumors.

In vivo efficacy of Hsp90 inhibition and PD-1 blockade in an orthotopic PDAC model

The efficacy of combined therapy with XL888 and anti–PD-1 Ab was next examined in a more aggressive and physiologically relevant murine model. Luciferase-expressing KPC tumor cells (KPC-Luc) were orthotopically implanted into the pancreas of immune-competent C57BL/6 mice. This model better recapitulates the stromal reaction evident in the pancreas. Seven days following injection, the presence of pancreatic tumors was confirmed via BLI in mice, and treatment was initiated (**Fig. 4D**). Tumor-bearing mice treated with

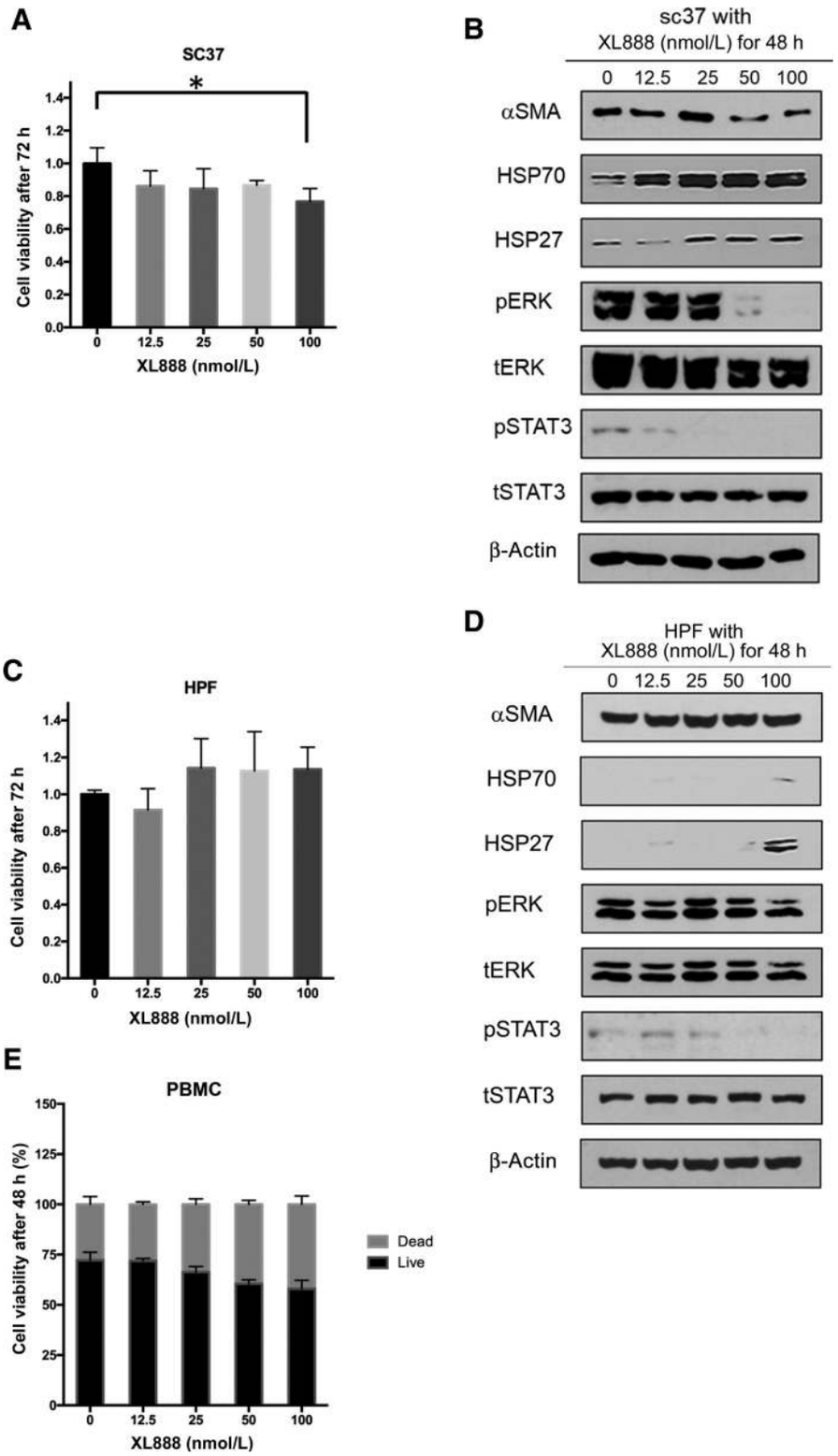

Figure 2.

Effect of Hsp90 inhibition on primary PSC/CAF and normal pancreatic fibroblasts. Treatment of primary PDAC patient–derived PSC/CAF (SC37) or normal HPFs with XL888 was analyzed by MTT assay (**A** and **C**) following a 72-hour treatment or immunoblot analysis (**B** and **D**) following a 48-hour treatment. β-Actin served as a loading control. *, $P < 0.05$. **E,** Analysis of Trypan blue staining of PBMCs from normal donors following a 48-hour treatment with XL888. Error bars, SD of $n = 3$ biological replicates.

anti–PD-1 Ab alone or the combination had a trend toward a lower rate of change in BLI signal over time, but these data were not statistically significant (Supplementary Fig. S5). Importantly, the body weight of mice in this model was also stable, indicative of a well-tolerated treatment regimen (**Fig. 4E**). Although useful, BLI signals have inherent limitations as a surrogate of tumor growth given the

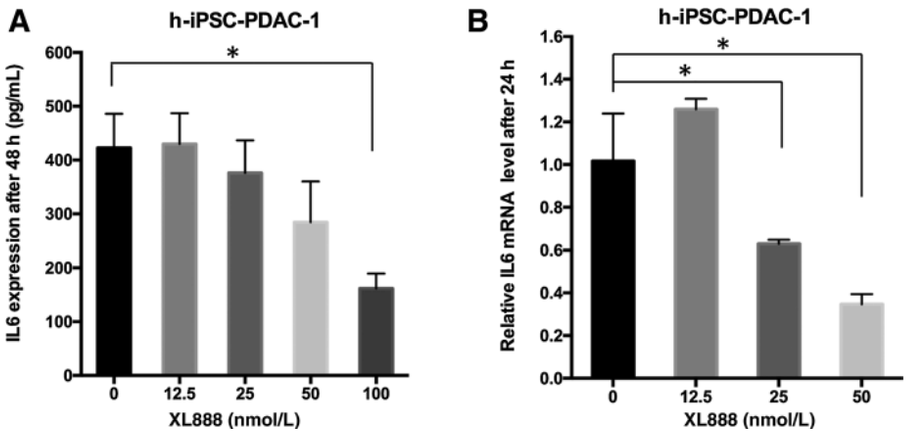

Figure 3.

Modulation of PSC/CAF-derived IL6 by Hsp90 inhibition. **A,** Reduced secretion of IL6 in culture supernatants from an immortalized PDAC-derived human PSC/CAF (h-iPSC-PDAC-1) following a 48-hour treatment with XL888. **B,** Real-time PCR for IL6 transcript was conducted on RNA isolated from h-iPSC-PDAC-1 following 24-hour treatment with XL888. Data were normalized to GAPDH as a housekeeping gene and expressed relative to cells treated with vehicle. Error bars, SD of $n = 3$ biological replicates; *, $P < 0.05$.

potential impact of subtle differences in anatomic tumor location and other factors including tissue necrosis. To better examine impact on tumor burden in the pancreas, tumor weight was also obtained post-mortem at the study endpoint on all animals. Results confirmed significantly lower tumor weights in mice treated with XL888 and anti–PD-1 Ab combined as compared with isotype control and those receiving XL888 alone ($P < 0.05$; **Fig. 4F**).

Combined XL888 and anti–PD-1 reprogram the TME

To understand the mechanism by which XL888 treatment enhanced the efficacy of anti–PD-1 therapy, histologic interrogation of the TME was also conducted in tumors obtained at the study endpoint. Reduced αSMA staining was observed in mice receiving anti–PD-1 Ab alone or combined with XL888, as compared with mice treated with isotype control Ab and vehicle ($P < 0.05$; **Fig. 5A**). In addition to this impact of therapy upon the PDAC stroma, other mechanisms may also be operative. Indeed, *in vitro* studies confirmed that XL888 had direct antiproliferative action upon KPC-Luc and other murine PDAC cell lines (Supplementary Fig. S4B–S4D). Analysis of pSTAT3 showed a trend toward reduced expression in tumors from mice receiving XL888 as a single agent ($P = 0.08$) or a significant decrease in pSTAT3 when XL888 was combined with anti–PD-1 Ab ($P < 0.05$; **Fig. 5B**). Surprisingly, single-agent PD-1 treatment was also associated with significantly reduced pSTAT3 in tumor tissue as compared with tumors from control mice in this tumor model ($P < 0.05$; **Fig. 5B**). Strikingly, both $CD8^+$ and $CD4^+$ T-cell infiltration was significantly increased in tumors from mice receiving XL888 combined with anti–PD-1 Ab ($P < 0.05$; **Fig. 5C** and **D**). Contrasting these data were no significant difference in the presence of B cells ($B220^+$), dendritic cells ($CD11c^+$), macrophages ($F4/80^+$), or phenotypically defined T regulatory cells ($CD4^+FoxP3^+$) between groups (Supplementary Fig. S6). In an effort to uncover global changes in immune-related gene expression unique to tumors in mice receiving the combination of XL888 and anti–PD-1 Ab, RNA was isolated from tumors and subjected to nanostring analysis using the nCounter Nanostring PanCancer Immune Profiling Panel. A unique pattern of gene expression was evident in tumors from mice treated with anti–PD-1, XL888, or both agents combined when compared with tumors from vehicle-treated mice (**Fig. 6A**). In fact, very little overlap was observed, with only 2 differentially expressed genes shared between the anti–PD-1 and combination groups. Of the genes differentially expressed in tumors from mice receiving combined XL888 and anti–PD-1 therapy, many of those upregulated were involved in immune response (e.g., IL21, S100a8, IL12Rβ1, CFi) and chemotaxis (CXCL13, CXCR2, and CCL24). In contrast, fewer genes involved in immune response were differentially expressed in tumors from mice treated with anti–PD-1 (downregulation of CCL17) or XL888 (upregulation of IL15 and CCL25) as compared with controls (**Fig. 6B** and **C**).

Discussion

This report describes how inhibition of Hsp90 affects PSC/CAF and enhances the efficacy of PD-1 blockade *in vivo*. We utilized a combination of immortalized cell lines, cell cultures derived from primary patient specimens, and *in vivo* models to interrogate the mechanism of this combined therapeutic approach on tumor growth and immune modulation. These data represent the first report of Hsp90 as a mediator of an activated phenotype of PSC/CAF, and the efficacy of a novel combination therapy approach in the setting of PDAC. Our results complement prior published reports showing direct growth-inhibitory and proapoptotic effects against pancreatic cancer cells (20, 31–38) and broaden our understanding of PSC/CAF as potential cellular targets of a clinically relevant Hsp90 inhibitor.

Hsp90 is important in regulating PDAC growth and survival; however, its role in PSC/CAF has not been investigated to date. Hsp90 cooperates with STAT3, NF-kB, and other factors to facilitate a paracrine circuit of cytokines that fuels inflammatory changes in PDAC (18–20). These cytokine changes are likely regulated in both the tumor and stromal cell compartments. Our data indicate that XL888 can modulate the activation of PSC/CAF, which in turn may shape the downstream immune response. These data suggest further study into how modulation of PSC/CAF biology and subsequent changes in downstream cytokine mediators might shape the immune contexture of the PDAC TME. For example, prior studies indicate that IL1α secreted from PDAC tumor cells fuels an inflammatory, IL6-producing subpopulation of CAF (10). Another report has implicated PSC-derived leukemia-inhibitory factor (LIF) as an upstream factor ultimately responsible for IL-6 production from these same cells (11, 13, 14). Although LIF was produced by the h-iPSC-PDAC-1 cell line and decreased following XL888 treatment (Supplementary Fig. S2), its secretion was not detected from all patient-derived PSC/CAF cultures. The specific contribution of downregulated factors such as IL6, in response to XL888, will be of interest in future studies.

In contrast to other solid tumors, targeting the PD-1/PD-L1 pathway has not affected the clinical course of disease in PDAC. This is likely due to a redundant series of immunosuppressive mechanisms that limit T-cell access into tumors, while suppressing their survival and function should they exhibit reactivity to tumor antigens in the

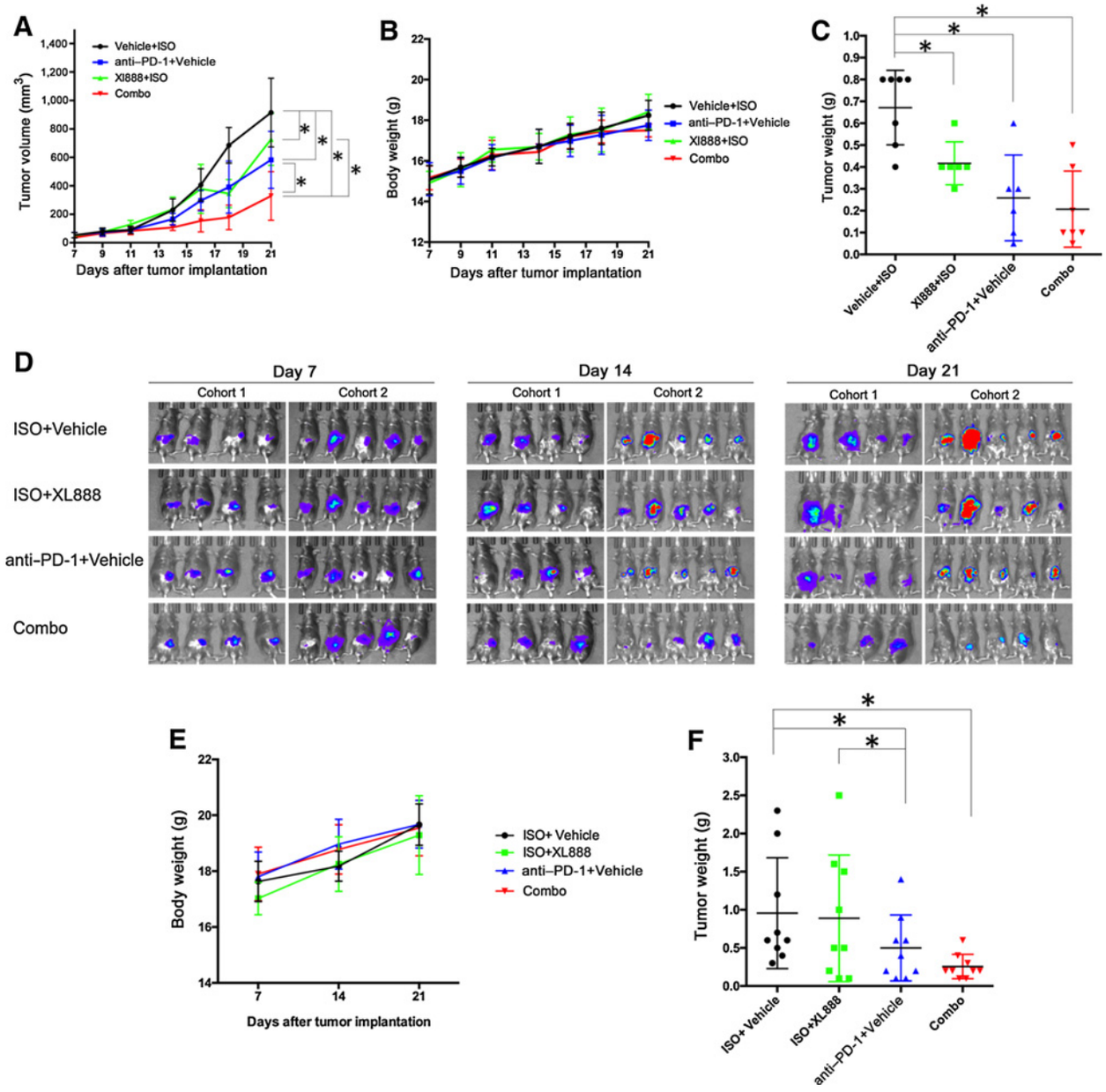

Figure. 4.

In vivo activity of XL888 and anti–PD-1. **A,** Tumor volume was measured over time in mice bearing subcutaneous panc02 tumors. Treatment started on day 7 once tumors were palpable. **B,** Body weight over time. Error bars, SD from $n = 6$ to 7 mice per group. **C,** End study tumor weight from each animal. Each dot represents an individual mouse tumor with the bar representing the mean. *A mixed model with pairwise comparisons revealed $P < 0.0001$ in combination therapy vs. the three other groups. **D,** BLI of mice confirming implantation of luciferase expressing KPC cells at day 7 after tumor implantation and at various time points during the study. Treatment was initiated on day 7 following tumor implantation and continued to the study endpoint at day 21. This study was conducted in two separate cohorts of mice, as displayed. Body weight over time (**E**) and end study tumor weight (**F**) from each animal. Each dot represents an individual mouse tumor with the bar representing the mean. Error bars, SD from $n = 9$ mice per treatment group. ISO, isotype control Ab.

microenvironment. The PDAC stroma is gaining appreciation as a factor that limits efficacy of immune checkpoint blockade in this disease (3, 27, 39–42). Therefore, therapies intended to inhibit stromal targets are a topic of great interest and may lend to increasing sensitivity to immune therapy approaches. For example, targeting FAP^+ fibroblasts in PDAC enhances the efficacy of immune checkpoint blockade in preclinical models. PSC/CAF certainly secrete abundant cytokines such as IL6 that act via STAT3 to expand myeloid-derived suppressor cells (12). Aligned with these data are further studies indicating that Ab-mediated blockade of IL6 increases tumoral infiltration of effector T cells and enhances the efficacy of immune checkpoint blockade in preclinical models of PDAC (27).

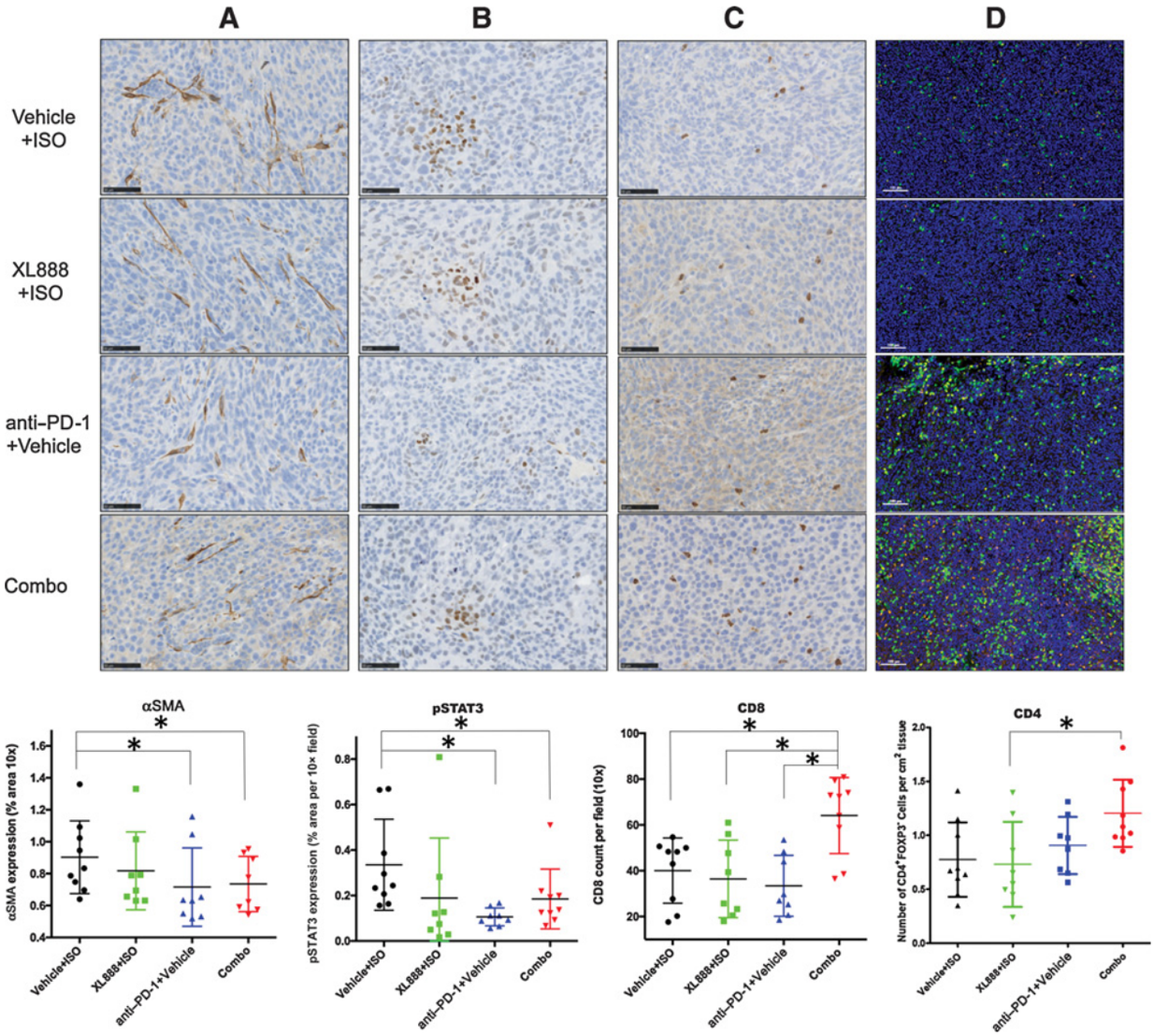

Figure 5.

Analysis of IHC data from orthotopic tumor study. Representative analysis and data summary of IHC for (**A**) αSMA, (**B**) pSTAT3, and (**C**) $CD8^+$ T-cell infiltration in orthotopic tumors obtained from mice at the study endpoint. **D,** Representative multiparameter immunofluorescence staining and data summary for $CD4^+$ $FoxP3^-$ cell infiltration in tumors obtained from mice at the study endpoint. Each dot represents an individual mouse tumor with the bar representing the mean percentage of positively stained area (for αSMA and pSTAT3) or mean number of positive cells per 10× field counted.

This adaptation of Hsp90 inhibition in preclinical models of PDAC in the present study provided a similar result, whereby PSC/CAF-derived production of IL6 was attenuated and infiltration of both $CD4^+$ and $CD8^+$ T cells was prominent in tumors from mice treated with the combination of XL888 and anti–PD-1 Abs. Given that PSC/CAF are exquisitely sensitive to STAT3 inhibitors (43), it is likely that interactions between Hsp90, STAT3, and other key prosurvival pathways influenced by its chaperone activity contribute to regulating viability and cytokine production by inflammatory fibroblasts in the PDAC TME, thereby rendering a tumor more permissive to T cells.

Inhibition of Hsp90 may enhance the efficacy of PD-1/PD-L1 pathway blockade through several mechanisms. Our data substantiate immune modulation as one viable contributor to antitumor activity. We saw that T-cell infiltration was accompanied by increased expression of genes encoding chemokine and chemokine receptors in tumors from mice receiving combination therapy. Although these data may simply reflect an increased proportion of T cells in tumors, they may also signify treatment-induced changes in Hsp90 client proteins such as NF-κB or Jak/STAT signaling intermediates that regulate expression of chemokines or their receptors at the transcriptional level. Given the number of client proteins for Hsp90, it is most likely that multiple concurrent mechanisms are operative when inhibitors of this pathway are combined with targeting PD-1/PD-L1. For instance, XL888 and other Hsp90 inhibitors such as ganetespib (20, 31–38) can directly inhibit growth (Supplementary Figs. S3 and S4) and modulate epigenetic properties of pancreatic cancer cells. These same downstream effects may in fact be relevant to immune cells as well and will be a continued topic of investigation. Certainly, Hsp90 plays a complicated

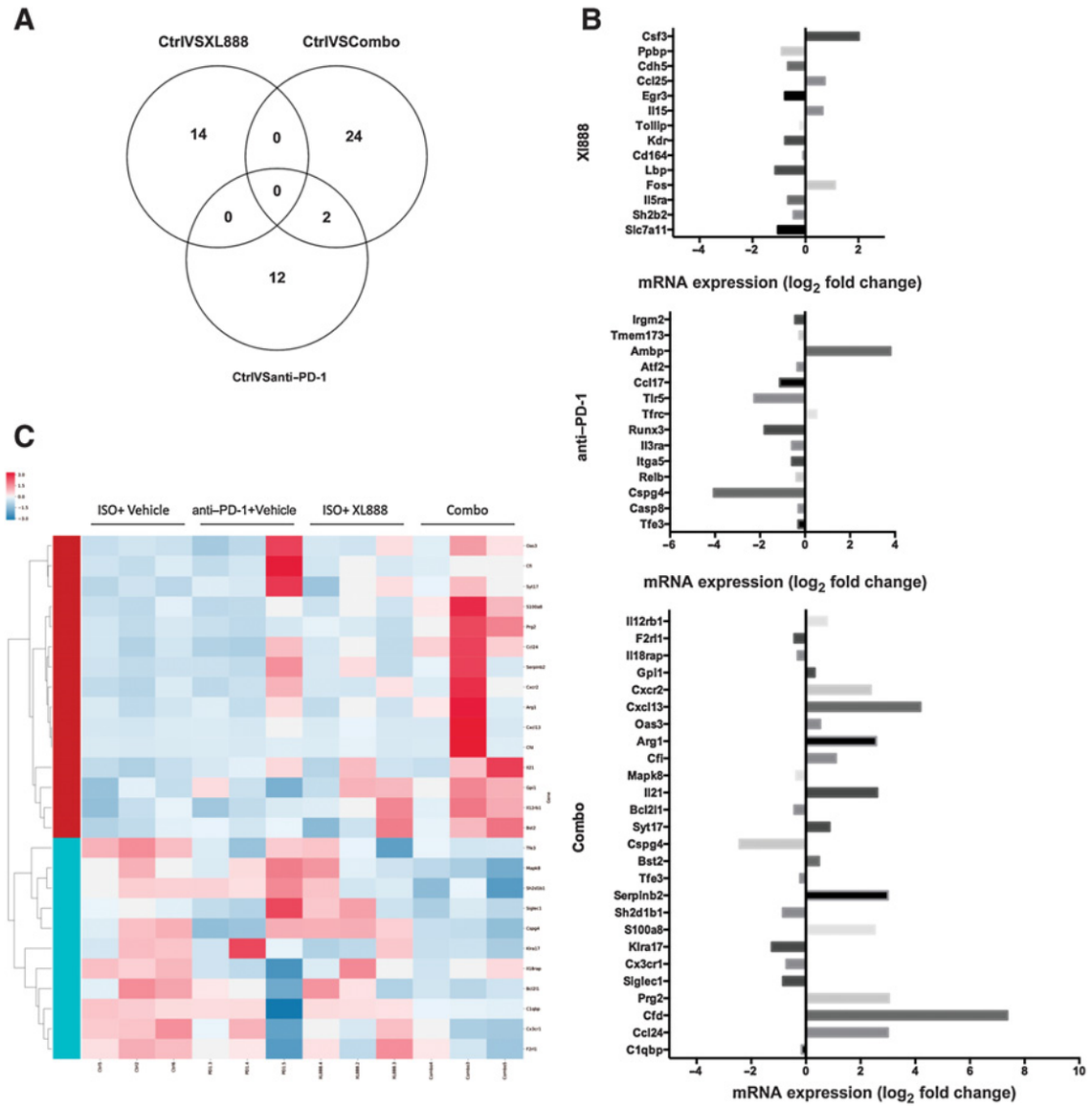

Figure 6.

Differential gene expression in orthotopic tumors from mice treated with combined XL888 and anti–PD-1 Ab. Analysis of gene expression differences was conducted using the nCounter Nanostring PanCancer Immune Profiling Panel. **A,** Venn diagram indicating the number of differentially expressed genes was found in each comparison of treatment groups, and how many genes overlapped within each set of comparisons. **B,** Heat map clustering of gene expression derived from tumors in each treatment group. Unsupervised hierarchical clustering of genes and samples was carried out by uncentered Pearson correlation. Color indicated normalized counts of each gene, with red representing higher expression and green relatively lower expression. **C,** Summary of differentially expressed genes expressed as $\log_2$ fold change in mRNA expression between control mice (treated with ISO + vehicle) as compared with each individual treatment group.

role as a regulator of immune responses. Although a subset of studies suggest Hsp90 inhibitors may antagonize T-cell–mediated immune responses by virtue of decreasing dendritic cell maturation (44, 45), or may negatively regulate CD28 expression, a key costimulatory pathway required for full reversal of exhausted T cells (44, 46–48), other studies instead show Hsp90 inhibition can alter cells in a manner that promotes tumor antigenicity and T-cell trafficking (16). Consistent with our data are prior *in vivo* studies demonstrating that a separate Hsp90 inhibitor, ganetespib, augments the antitumor activity of PD-1 blockade in subcutaneous MC38 colon and B16 melanoma models (49) and CTLA-4 blockade in MC38 colon models by eliciting IFN-stimulated gene signatures (50). These results highlight the need for additional data to assess the immunomodulatory properties of Hsp90 inhibitors in the context of immune checkpoint blockade.

Although our results are promising, a number of limitations deserve mention that are relevant in the context of interpreting the data. First, PSC/CAF by their nature are inherently heterogeneous and capable of phenotypic plasticity. Thus, the data obtained in two-dimensional, *in vitro* culture models may not fully

recapitulate what might be seen in a spheroid culture, or most importantly, a patient tumor. Second, our data are limited to pharmacologic inhibition rather than genetic ablation of the pathway as a complementary approach. Unfortunately, we did not choose this methodology given prior reports that Hsp90α and Hsp90β isoforms can compensate for one another. These factors would make interpretation of our results quite complex. Furthermore, our data implicating a role for Hsp90 in cell compartments outside of only tumor cells (i.e., PSC/CAF and possibly immune cells) would render it difficult to achieve precise genetic modulation in one cell type. In this scenario, the use of a targeted inhibitor was the most efficient way to approach this study. Finally, the XL888 Hsp90 inhibitor is a next-generation compound that our group is currently utilizing in an ongoing phase Ib/II clinical trial of XL888 combined with pembrolizumab in patients with advanced pancreatic and colorectal cancer (NCT3095781). This study also has a robust series of laboratory correlative studies that will be informative related to its mechanism of action in the clinical setting.

Overall, the application of combining targeted, small-molecule inhibitors with immunotherapy approaches in the setting of PDAC is an area of high priority for overcoming limited efficacy. In addition, the development and refinement of next-generation, small-molecule Hsp90 inhibitors are areas of continued interest to simultaneously modulate inflammatory pathways across multiple cell compartments. We are hopeful that data from our preclinical and clinical work with XL888 may inform other studies using this class of agents in the future, with the goal of enhancing efficacy of immunotherapy and modulating the PDAC stroma.

Authors' Disclosures

B.M. Olson reports grants from Boehringer Ingelheim RCV GmbH & Co KG, grants from Vaccinex, Inc. outside the submitted work, and a patent for McNeel D and Olson B. US patent no. 10561716 B2 (prostate cancer vaccine issued, licensed, and with royalties paid from Madison Vaccine, Inc.) and a patent for McNeel D and Olson B. US patent no. 20170354725A1 (combinatorial androgen deprivation with an androgen receptor vaccine) pending (filed by Wisconsin Alumni Research Foundation). R. Ahmed reports a patent for PD-1 with royalties paid (Genentech). B.F. El-Rayes reports grants from Novartis (clinical trial), Merck (clinical trial), Boston Biomedical (clinical trial), Pfizer (clinical trial), Bayer (clinical trial), Xencor (clinical trial), Adaptamune (clinical trial), EUSA (clinical trial), and AstraZeneca (clinical trial); personal fees from Merck (advisory board), Ipsen (advisory board), Natera (advisory board), BMS (advisory board), Exelixis (DSMB), and Erytech (DSMB) outside the submitted work; B.F. El-Rayes also serves as a consultant to Merck and receives compensation for these services. The terms of this arrangement have been reviewed and approved by Emory University in accordance with its conflict of interest policies. G.B. Lesinski reports grants from NCI during the conduct of the study, as well as other from ProDa Biotech, LLC (consulting), Merck and Co. (sponsored research agreement through Emory University), Bristol-Myers Squibb (sponsored research agreement through Emory University), Boehringer Ingelheim (sponsored research agreement through Emory University), and Vaccinex (sponsored research agreement through Emory University) outside the submitted work. No disclosures were reported by the other authors.

Authors' Contributions

Y. Zhang: Formal analysis, investigation, methodology, writing-original draft, writing-review and editing. **M.B. Ware:** Conceptualization, data curation, formal analysis, investigation, methodology, writing-original draft, writing-review and editing. **M.Y. Zaidi:** Formal analysis, investigation, writing-original draft, writing-review and editing. **A.N. Ruggieri:** Formal analysis, investigation, methodology, writing-review and editing. **B.M. Olson:** Investigation, writing-review and editing. **H. Komar:** Supervision, investigation, writing-review and editing. **M.R. Farren:** Supervision, investigation, writing-review and editing. **G.P. Nagaraju:** Conceptualization, investigation, writing-review and editing. **C. Zhang:** Data curation, formal analysis, writing-review and editing. **Z. Chen:** Data curation, formal analysis, supervision, writing-original draft, writing-review and editing. **J.M. Sarmiento:** Resources, investigation, writing-review and editing. **R. Ahmed:** Conceptualization, writing-original draft, writing-review and editing. **S.K. Maithel:** Resources, writing-original draft, writing-review and editing. **B.F. El-Rayes:** Conceptualization, formal analysis, supervision, funding acquisition, investigation, writing-original draft, project administration, writing-review and editing. **G.B. Lesinski:** Conceptualization, resources, formal analysis, supervision, funding acquisition, validation, investigation, writing-original draft, project administration, writing-review and editing.

Acknowledgments

Research reported in this publication was supported in part by the Biostatistics and Bioinformatics, Integrated Cell Imaging, Pathology Shared Resources of Winship Cancer Institute of Emory University and NIH/NCI under award number P30CA138292. This study was also supported by NIH grants 1R01CA228406-01A1 and P30CA138292.

We also acknowledge the contribution of the Emory Integrated Genomics Core (EIGC), which is subsidized by the Emory University School of Medicine and is one of the Emory Integrated Core Facilities. The content is solely the responsibility of the authors and does not necessarily represent the official views of the NIH.

The costs of publication of this article were defrayed in part by the payment of page charges. This article must therefore be hereby marked *advertisement* in accordance with 18 U.S.C. Section 1734 solely to indicate this fact.

Received September 19, 2019; revised April 9, 2020; accepted September 30, 2020; published first October 9, 2020.

References

1. Siegel RL, Miller KD, Jemal A. Cancer statistics, 2020. CA Cancer J Clin 2020;70:7–30.
2. Rahib L, Smith BD, Aizenberg R, Rosenzweig AB, Fleshman JM, Matrisian LM. Projecting cancer incidence and deaths to 2030: the unexpected burden of thyroid, liver, and pancreas cancers in the United States. Cancer Res 2014;74:2913–21.
3. Neesse A, Michl P, Frese KK, Feig C, Cook N, Jacobetz MA, et al. Stromal biology and therapy in pancreatic cancer. Gut 2011;60:861–8.
4. Apte MV, Haber PS, Applegate TL, Norton ID, McCaughan GW, Korsten MA, et al. Periacinar stellate shaped cells in rat pancreas: identification, isolation, and culture. Gut 1998;43:128–33.
5. Krizhanovsky V, Yon M, Dickins RA, Hearn S, Simon J, Miething C, et al. Senescence of activated stellate cells limits liver fibrosis. Cell 2008;134:657–67.
6. Lonardo E, Frias-Aldeguer J, Hermann PC, Heeschen C. Pancreatic stellate cells form a niche for cancer stem cells and promote their self-renewal and invasiveness. Cell Cycle 2012;11:1282–90.
7. Waghray M, Yalamanchili M, di Magliano MP, Simeone DM. Deciphering the role of stroma in pancreatic cancer. Curr Opin Gastroen 2013;29:537–43.
8. Moffitt RA, Marayati R, Flate EL, Volmar KE, Loeza SG, Hoadley KA, et al. Virtual microdissection identifies distinct tumor- and stroma-specific subtypes of pancreatic ductal adenocarcinoma. Nat Genet 2015;47:1168–78.
9. Ohlund D, Handly-Santana A, Biffi G, Elyada E, Almeida AS, Ponz-Sarvise M, et al. Distinct populations of inflammatory fibroblasts and myofibroblasts in pancreatic cancer. J Exp Med 2017;214:579–96.
10. Biffi G, Oni TE, Spielman B, Hao Y, Elyada E, Park Y, et al. IL1-induced JAK/STAT signaling is antagonized by TGFbeta to shape CAF heterogeneity in pancreatic ductal adenocarcinoma. Cancer Discov 2019;9:282–301.
11. Bressy C, Lac S, Nigri J, Leca J, Roques J, Lavaut MN, et al. LIF drives neural remodeling in pancreatic cancer and offers a new candidate biomarker. Cancer Res 2018;78:909–21.
12. Mace TA, Ameen Z, Collins A, Wojcik S, Mair M, Young GS, et al. Pancreatic cancer-associated stellate cells promote differentiation of myeloid-derived suppressor cells in a STAT3-dependent manner. Cancer Res 2013;73:3007–18.
13. Shi Y, Gao W, Lytle NK, Huang P, Yuan X, Dann AM, et al. Targeting LIF-mediated paracrine interaction for pancreatic cancer therapy and monitoring. Nature 2019;569:131–5.

14. Wang MT, Fer N, Galeas J, Collisson EA, Kim SE, Sharib J, et al. Blockade of leukemia inhibitory factor as a therapeutic approach to KRAS driven pancreatic cancer. Nat Commun 2019;10:3055.
15. Taipale M, Jarosz DF, Lindquist S. HSP90 at the hub of protein homeostasis: emerging mechanistic insights. Nat Rev Mol Cell Biol 2010;11:515–28.
16. Graner MW. HSP90 and immune modulation in cancer. Adv Cancer Res 2016; 129:191–224.
17. Haggerty TJ, Dunn IS, Rose LB, Newton EE, Pandolfi F, Kurnick JT. Heat shock protein-90 inhibitors enhance antigen expression on melanomas and increase T cell recognition of tumor cells. PLoS One 2014;9:e114506.
18. Rao A, Taylor JL, Chi-Sabins N, Kawabe M, Gooding WE, Storkus WJ. Combination therapy with HSP90 inhibitor 17-DMAG reconditions the tumor microenvironment to improve recruitment of therapeutic T cells. Cancer Res 2012;72:3196–206.
19. Noman MZ, Desantis G, Janji B, Hasmim M, Karray S, Dessen P, et al. PD-L1 is a novel direct target of HIF-1alpha, and its blockade under hypoxia enhanced MDSC-mediated T cell activation. J Exp Med 2014;211:781–90.
20. Nagaraju GP, Park W, Wen J, Mahaseth H, Landry J, Farris AB, et al. Anti-angiogenic effects of ganetespib in colorectal cancer mediated through inhibition of HIF-1alpha and STAT-3. Angiogenesis 2013;16:903–17.
21. Bussenius J, Blazey CM, Aay N, Anand NK, Arcalas A, Baik T, et al. Discovery of XL888: a novel tropane-derived small molecule inhibitor of HSP90. Bioorg Med Chem Lett 2012;22:5396–404.
22. Neckers L, Blagg B, Haystead T, Trepel JB, Whitesell L, Picard D. Methods to validate Hsp90 inhibitor specificity, to identify off-target effects, and to rethink approaches for further clinical development. Cell Stress Chaperones 2018;23: 467–82.
23. Pedersen KS, Kim GP, Foster NR, Wang-Gillam A, Erlichman C, McWilliams RR. Phase II trial of gemcitabine and tanespimycin (17AAG) in metastatic pancreatic cancer: a Mayo Clinic Phase II Consortium study. Invest New Drugs 2015;33:963–8.
24. Ma Y, Hwang RF, Logsdon CD, Ullrich SE. Dynamic mast cell-stromal cell interactions promote growth of pancreatic cancer. Cancer Res 2013;73: 3927–37.
25. Komar HM, Serpa G, Kerscher C, Schwoegl E, Mace TA, Jin M, et al. Inhibition of Jak/STAT signaling reduces the activation of pancreatic stellate cells in vitro and limits caerulein-induced chronic pancreatitis in vivo. Sci Rep 2017;7:1787.
26. Lechner MG, Liebertz DJ, Epstein AL. Characterization of cytokine-induced myeloid-derived suppressor cells from normal human peripheral blood mononuclear cells. J Immunol 2010;185:2273–84.
27. Mace TA, Shakya R, Pitarresi JR, Swanson B, McQuinn CW, Loftus S, et al. IL-6 and PD-L1 antibody blockade combination therapy reduces tumour progression in murine models of pancreatic cancer. Gut 2016;67:320–32.
28. McQuin C, Goodman A, Chernyshev V, Kamentsky L, Cimini BA, Karhohs KW, et al. CellProfiler 3.0: next-generation image processing for biology. PLoS Biol 2018;16:e2005970.
29. Lamprecht MR, Sabatini DM, Carpenter AE. CellProfiler: free, versatile software for automated biological image analysis. BioTechniques 2007;42: 71–5.
30. Bankhead P, Loughrey MB, Fernandez JA, Dombrowski Y, McArt DG, Dunne PD, et al. QuPath: open source software for digital pathology image analysis. Sci Rep 2017;7:16878.
31. Adachi S, Yasuda I, Nakashima M, Yamauchi T, Yamauchi J, Natsume H, et al. HSP90 inhibitors induce desensitization of EGF receptor via p38 MAPK-mediated phosphorylation at Ser1046/1047 in human pancreatic cancer cells. Oncol Rep 2010;23:1709–14.
32. Moser C, Lang SA, Hackl C, Wagner C, Scheiffert E, Schlitt HJ, et al. Targeting HSP90 by the novel inhibitor NVP-AUY922 reduces growth and angiogenesis of pancreatic cancer. Anticancer Res 2012;32:2551–61.
33. Nagaraju GP, Mezina A, Shaib WL, Landry J, El-Rayes BF. Targeting the Janus-activated kinase-2-STAT3 signalling pathway in pancreatic cancer using the HSP90 inhibitor ganetespib. Eur J Cancer 2016;52:109–19.
34. Nagaraju GP, Wu C, Merchant N, Chen Z, Lesinski GB, El-Rayes BF. Epigenetic effects of inhibition of heat shock protein 90 (HSP90) in human pancreatic and colon cancer. Cancer Lett 2017;402:110–6.
35. Nagaraju GP, Zakka KM, Landry JC, Shaib WL, Lesinski GB, El-Rayes BF. Inhibition of HSP90 overcomes resistance to chemotherapy and radiotherapy in pancreatic cancer. Int J Cancer 2019;145:1529–37.
36. Song D, Chaerkady R, Tan AC, Garcia-Garcia E, Nalli A, Suarez-Gauthier A, et al. Antitumor activity and molecular effects of the novel heat shock protein 90 inhibitor, IPI-504, in pancreatic cancer. Mol Cancer Ther 2008;7:3275–84.
37. Xue N, Jin J, Liu D, Yan R, Zhang S, Yu X, et al. Antiproliferative effect of HSP90 inhibitor Y306zh against pancreatic cancer is mediated by interruption of AKT and MAPK signaling pathways. Curr Cancer Drug Targets 2014;14:671–83.
38. Zhang T, Hamza A, Cao X, Wang B, Yu S, Zhan CG, et al. A novel Hsp90 inhibitor to disrupt Hsp90/Cdc37 complex against pancreatic cancer cells. Mol Cancer Ther 2008;7:162–70.
39. Blair AB, Kim VM, Muth ST, Saung MT, Lokker N, Blouw B, et al. Dissecting the stromal signaling and regulation of myeloid cells and memory effector T cells in pancreatic cancer. Clin Cancer Res 2019;25:5351–63.
40. Fearon DT. The carcinoma-associated fibroblast expressing fibroblast activation protein and escape from immune surveillance. Cancer Immunol Res 2014;2: 187–93.
41. Feig C, Jones JO, Kraman M, Wells RJ, Deonarine A, Chan DS, et al. Targeting CXCL12 from FAP-expressing carcinoma-associated fibroblasts synergizes with anti-PD-L1 immunotherapy in pancreatic cancer. Proc Natl Acad Sci USA 2013; 110:20212–7.
42. Lo A, Wang LC, Scholler J, Monslow J, Avery D, Newick K, et al. Tumor-promoting desmoplasia is disrupted by depleting FAP-expressing stromal cells. Cancer Res 2015;75:2800–10.
43. Mace TA, Bloomston M, Lesinski GB. Pancreatic cancer-associated stellate cells: a viable target for reducing immunosuppression in the tumor microenvironment. Oncoimmunology 2013;2:e24891.
44. Bae J, Munshi A, Li C, Samur M, Prabhala R, Mitsiades C, et al. Heat shock protein 90 is critical for regulation of phenotype and functional activity of human T lymphocytes and NK cells. J Immunol 2013;190:1360–71.
45. Trojandt S, Reske-Kunz AB, Bros M. Geldanamycin-mediated inhibition of heat shock protein 90 partially activates dendritic cells, but interferes with their full maturation, accompanied by impaired upregulation of RelB. J Exp Clin Cancer Res 2014;33:16.
46. Schnaider T, Somogyi J, Csermely P, Szamel M. The Hsp90-specific inhibitor, geldanamycin, blocks CD28-mediated activation of human T lymphocytes. Life Sci 1998;63:949–54.
47. Kelly PN. CD28 is a critical target for PD-1 blockade. Science 2017;355:1386.
48. Kamphorst AO, Wieland A, Nasti T, Yang S, Zhang R, Barber DL, et al. Rescue of exhausted CD8 T cells by PD-1-targeted therapies is CD28-dependent. Science 2017;355:1423–7.
49. Proia DA, Kaufmann GF. Targeting heat-shock protein 90 (HSP90) as a complementary strategy to immune checkpoint blockade for cancer therapy. Cancer Immunol Res 2015;3:583–9.
50. Mbofung RM, McKenzie JA, Malu S, Zhang M, Peng W, Liu C, et al. HSP90 inhibition enhances cancer immunotherapy by upregulating interferon response genes. Nat Commun 2017;8:451.